Available online at www.sciencedirect.com
ScienceDirect
Ceramics International 37 (2011) 3565–3573
CERAMICS INTERNATIONAL
www.elsevier.com/locate/ceramint

Effects of the nature of the doping salt and of the thermal pre-treatment and sintering temperature on Spark Plasma Sintering of transparent alumina

Nicolas Roussel [a], Lucile Lallemant [b,c], Bernard Durand [a,*], Sophie Guillemet [a], Jean-Yves Chane Ching [a], Gilbert Fantozzi [b,c], Vincent Garnier [b,c], Guillaume Bonnefont [b,c]

[a] CIRIMAT, UMR CNRS 5085, Université Paul Sabatier – 118 route de Narbonne – F-31062 TOULOUSE Cedex 9, France
[b] Université de Lyon, CNRS, France
[c] INSA-Lyon, MATEIS UMR5510, F-69621 Villeurbanne, France

Received 20 April 2011; received in revised form 18 May 2011; accepted 24 May 2011
Available online 1 July 2011

Abstract

A slurry of α-Al_2O_3 was doped with Mg, Zr and La nitrates or chlorides, in various amounts in the range 150–500 wt ppm and then freeze-dried to produce nanosized doped powder (~150 nm). The powder was sintered by SPS to yield transparent polycrystalline alpha alumina. The influence of the nature of the doping element and the starting salt, the thermal treatment before sintering and the sintering temperature on the transparency of the ceramics were investigated. The transparency of the ceramics of nanosized Al_2O_3 was shown to depend mainly on the way the powder was prepared, the nature of the doping salt also had an effect. Finally, a high real inline transmittance, reaching 48.1% was achieved after optimization.

Keywords: B. Grain size; B. Porosity; C. Optical properties; D. Al_2O_3; Doping; Spark Plasma Sintering

1. Introduction

For both mechanical and economical reasons, numerous studies have been performed over recent years to replace sapphire by transparent polycrystalline alumina (PCA) in various optical applications such as discharge lamp envelopes and optical windows or armour [1–5]. The light transmission properties of fine-grained PCA can be described by the Apetz and van Bruggen model [6], based on the Rayleigh-Gans-Debye approximation. The real inline transmittance (RIT) is strongly dependent on grain size (i.e. light scattering by grain boundaries γ_G) and porosity (i.e. light scattering by pores γ_p) as can be seen from the following equations:

$$\mathrm{RIT} = \frac{I_2}{I_1} = (1 - R_s) \cdot \exp(-\gamma_{\mathrm{tot}} \cdot D) \quad (1)$$

$$\gamma_{\mathrm{tot}} = \gamma_G + \gamma_p = \frac{3\pi^2 r \Delta n^2}{\lambda_0^2} + \frac{p}{\frac{4}{3}\pi \cdot r_p^3} \cdot C_{\mathrm{sca},p} \quad (2)$$

with I_1 and I_2 the light beam intensities before and after travelling through a sample of thickness D; R_s the total normal surface reflectance (=0.14 for PCA); γ_{tot} the total scattering coefficient; r the average grain radius; Δn the average refractive index change between two adjacent grains (=0.005 for PCA), λ_0 the wavelength of incident light under vacuum; p the total porosity, r_p the average pore radius and $C_{\mathrm{sca},p}$ the scattering cross section of one spherical pore [6,7]. As PCA is a birefringent material, the model predicts that to obtain high real in-line transmittance over the spectrum, both grain size (<0.5 μm) and porosity (<0.05% with a narrow distribution of nanometric pores) have to be carefully controlled. To do so, two strategies were combined: doping alumina with metal oxides (ppm range) and sintering the powders by Spark Plasma Sintering (SPS).

The effects of the doping elements on alumina have been studied for many years but are still the subject of diverse research. The first rule to control the densification of alumina is to start from a high purity powder. The process is very sensitive to impurities, especially silicon, calcium and sodium [8,9], which can lead to inhomogeneous densification with abnormal grain growth [9]. Small amounts of various doping oxides (MgO, La_2O_3, Y_2O_3) can be introduced in the alumina to have a better control of densification. Most of these doping agents, due

* Corresponding author. Tel.: +33 661 567 751; fax: +33 661 556 163.
E-mail address: bdurand@chimie.ups-tlse.fr (B. Durand).

0272-8842/$36.00
doi:10.1016/j.ceramint.2011.05.152

to their very low solubility in alumina, segregate at grain boundaries during the sintering. Some Secondary-Ion Mass Spectrometry (SIMS) images illustrate this phenomenon very clearly; after densification, the doping agent (MgO, La_2O_3 and Y_2O_3) is located at grain boundaries and pore surfaces [10,11]. For La_2O_3 and Y_2O_3 doping, the segregation leads to an inhibition of grain growth and decreases the densification rate [11]. The rate-controller, during sintering of fine alumina, was reported by some authors to be grain boundary diffusion [12–15]. Yoshida's group tried to explain how the doping elements act on grain boundary diffusivity. It is clear that the valence of the cation cannot explain this mechanism because Pt^{4+} increases the grain boundary diffusion while Zr^{4+} decreases it. According to the same authors, grain boundary diffusivity cannot be predicted by the size of the cation, but by ionicity in the vicinity of the grain boundaries. This ionicity improves the ionic bond strength and can limit atomic diffusion [16].

SPS is a processing technique that has been widely used over the past decades [1,5,17–20]. It was shown that dense, fine-grained materials can be developed at low temperatures and short sintering times compared to conventional techniques such as hot isostatic pressing (HIP). Grain growth is then significantly reduced. Several studies have been performed over recent years to obtain transparent alumina by SPS. The heating rate has been found to be a critical parameter in obtaining such a material. According to Aman et al. [20], grain-boundary diffusion probably dominates at low heating rates whereas grain coarsening, in respect of thermal equilibrium considerations, is unavoidable at high heating rates during the initial stages of low temperatures sintering. According to Kim et al. [1], when sintering at under 1250 °C, rapid heating creates high defect concentrations inducing dynamic grain growth and thus decreasing the transparency of the material. The in-line transmission of pure PCA was increased by about 15% (up to 46% at a wavelength of 640 nm) on decreasing the heating rate from 10 to 2 °C/min. Recently, Stuer et al. [5] increased the RIT of Spark Plasma Sintered PCA up to 57% at 640 nm, by tri-doping the powder with Mg, La and Y which proves the benefit of combining the strategy of doping with SPS. However, their RIT values are still far from those found by Krell et al. [2] using HIP (72% at 640 nm). Green body shaping was shown to be of crucial importance by Krell et al. [21] for natural sintering. Recently, Aman et al. [22] have shown that processing the green state also has a strong influence on the optical properties of Spark Plasma Sintered PCA. However, some aspects of the powder preparation such as the thermal treatment before sintering and the nature of the starting salt, have not been studied yet. The aim of this work is to give a basic overview of the powder preparation parameters which can play a role during the Spark Plasma Sintering of transparent PCA.

2. Experimental

The starting material was a commercial (BA15PSH, Baïkowski) high purity α-Al_2O_3 slurry (solid content 73.5 wt%) with a median particle size D_{50} of 150 nm. The total amount of impurity was less than 0.01 wt% (14 ppm Na, 60 ppm K, 7.1 ppm Fe, 13 ppm Si, 4 ppm Ca) as reported by the manufacturer.

The doping agents were introduced by weighing out the required amount of water-soluble salts (nitrates or chlorides) of lanthanum, zirconium and magnesium, pouring them into the alumina slurry and stirring for 24 h by rotation of the container. Then, the slurry was frozen in liquid nitrogen and freeze-dried for approximately 48 h (−40 °C, 0.1 mbar, Alpha2-4, Christ). The resulting powders were sintered either as-obtained or after thermal pre-treatment to transform the salt into oxide, at 450, 500 and 650 °C for Mg, Zr and La respectively, with no holding time.

The chosen doping agent amounts (wt ppm) were: 100, 200, 500 for ZrO_2, 100, 200, 500 for La_2O_3 and 150, 300, 500 for MgO. All ppm given in the following are expressed in weight.

Specific surface areas were measured by BET (Micromeritics FlowSorb II 2300), pore sizes were determined by mercury infiltration (Micromeritics Instrument Corp.) and TGA was performed using a Setaram TAG 24.

Densification was carried out by either conventional sintering or SPS. In the first case, 6 mm diameter pellets were uniaxially pressed at 200 MPa for 2 min and sintered in a conventional furnace at 1350 °C in static air for 2 h at a heating rate of 200 °C/h and then final densities were estimated from size and weight measurements. For SPS the powders were sieved (<500 μm) and sintered (HP D 25/1, FCT System, Rauenstein, Germany) using the following cycle: applied uniaxial pressure of 80 MPa throughout the cycle, rapid heating up to 800 °C, a heating rate of 10 °C/min from 800 °C to 1100 °C followed by a slower heating (1 °C/min) up to the final sintering temperature (T_f) in order to remove the residual porosity [1]. The final sintering temperature was in the range 1180–1280 °C. Rapid cooling ended the cycle, interrupted by a 10-min dwell at 1000 °C to release the residual stresses [1]. Then, the samples were carefully mirror-polished on both sides using diamond slurries and the transparency was evaluated by a real in-line transmittance (RIT) measurement (Jasco V-670) which only takes into account the unscattered light passing straight through the sample (i.e. the real transmitted light) as explained by Apetz and van Bruggen [6]. All the RIT values given in this paper were measured at λ = 640 nm and Eq. (3) was used to obtain the RIT at the same thickness of 0.88 mm to compare the results:

$$\mathrm{RIT}(t_2) = (1 - R_S)\left(\frac{\mathrm{RIT}(t_1)}{1 - R_S}\right)^{t_2/t_1} \quad (3)$$

where R_S is the total normal surface reflectance (=0.14 for PCA) and RIT (t_i) is the RIT for a sample of thickness t_i.

Setaram Setsys evolution TMA-16/18 was used to carry out dilatometric measurements in air with a heating rate of 2.5 °C/min and a final temperature of 1600 °C.

SEM Jeol JSM-6510LV and SEM Philips ESEM-FEG FEI XL30 were used to investigate the microstructure of the samples. The average line intercept method has been used to estimate grain sizes on fracture surfaces, applying a correction factor of 1.56 [23].

Table 1
RIT at 640 nm for 0.88 mm thick pellets and grain size of undoped ceramics sintered by SPS at different temperatures.

Sintering temperature (°C)	1280	1250	1230	1200	1180
RIT (%) (λ = 640 nm)	18.9	23	30.5	27.4	33.6
Grain size (μm)	1.93 ± 0.35	1.50 ± 0.23	1.17 ± 0.20	0.80 ± 0.19	0.52 ± 0.11

3. Results and discussion

3.1. Effect of sintering temperature and doping

As too high a temperature can cause grain growth during sintering, this parameter needs to be carefully controlled. Five samples of freeze dried pure alumina were sintered by SPS at different T_f (1180–1200–1230–1250–1280 °C). RIT and grain size were determined (Table 1). A maximum RIT of 33.6% was reached at 1180 °C. But at this temperature and at 1200 °C, a gradient of transparency was noted, indicating that the temperature was not the same at the centre (very dense and transparent) and at the edge (not dense and translucent) of the pellet [24–26]. The gradient was no longer observed for the sample sintered at 1230 °C which presented a high and homogeneous RIT of 30.5%. Moreover, when comparing the RIT all over the spectrum (300–2500 nm) (Fig. 1), it appears that the RIT of the sample sintered at 1180 °C was lower than that of the sample sintered at 1230 °C in the IR wavelengths (at λ = 2000 nm, RIT (1180 °C) = 64.9% and RIT (1230 °C) = 75.5%). The grain size of the ceramic increased regularly from 0.52 to 1.93 μm as the temperature was raised from 1180 to 1280 °C. This increase contributes to the decrease in RIT as the sintering temperature rises.

The measured RIT of samples sintered below 1230 °C were significantly lower than the theoretical values calculated for non-porous ceramics with the same grain size which corroborates the presence of residual porosity (Fig. 2). The RIT measured for ceramics sintered at 1230, 1250 and 1280 °C were very close to the theoretical ones, so 1230 °C can be considered as the optimized sintering temperature. The SEM micrographs (Fig. 3) show that the grain size in all undoped ceramic samples was not homogeneous. The sample sintered at 1230 °C, where the median grain size was 1.17 μm, exhibits grains with diameters ranging from 0.8 μm to 1.5 μm.

The grain size and the transparency of the pure alumina sintered at 1230 °C are in good agreement with the results found by Kim et al. [18]. When the temperature was decreased to 1150 °C, the transparency was improved in the visible range but decreased in the IR corroborating our results at 1180 °C. These authors were also able to increase the transparency of 30 mm diameter pellets sintered at 1150 °C up to 47% and decrease grain size to ∼300 nm [1,17]. However, these measurements were taken at the centre of the pellets. According to the same authors [18], rapid grain growth occurs in the centre of 30 mm diameter pellets compared to the outer part, probably resulting in inhomogeneous transparency of the samples. Decreasing the temperature is beneficial for a decrease in grain size and thus an increase in the RIT. But too low a temperature will lead to inhomogeneous samples. At low temperatures,

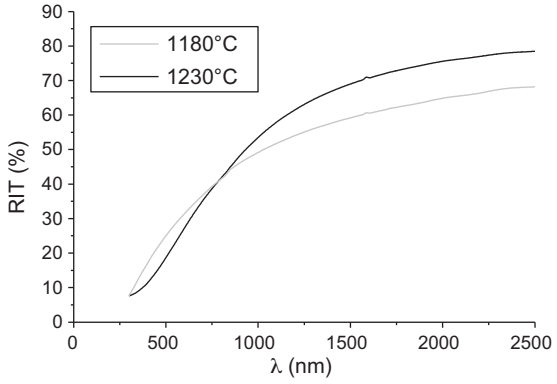

Fig. 1. Whole spectrum (300–2500 nm) RIT of two undoped alumina samples, sintered at 1180 °C (grey) and 1230 °C (black).

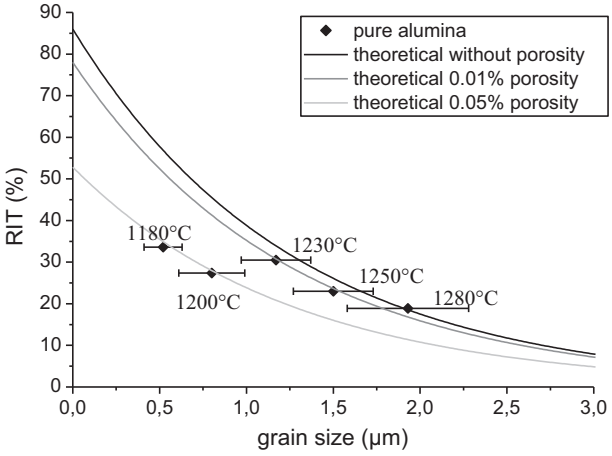

Fig. 2. Comparison of the RIT of pure alumina sintered by SPS with the theoretical curves (λ = 640 nm th = 0.88 mm).

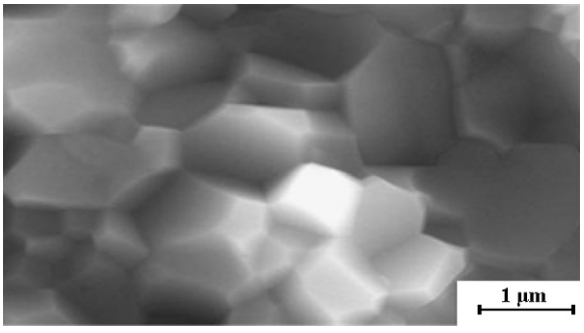

Fig. 3. SEM pictures of undoped alumina sintered by SPS at 1230 °C.

temperature gradient led to more porosity at the edge of the pellet explaining the loss of RIT. When increasing temperature, last porosities will shrink and an optimum between lower grain size with a higher amount of porosity at the edge and higher grain size with a lower amount of porosity at the centre will be found, explaining the homogenization of the RIT. Finally, when increasing again temperature, the same amount of porosity is found all over the sample. It means that the RIT difference is only due to grain size difference. This difference is decreasing when increasing grain size explaining why the samples are still homogeneous (Fig. 2). Optimizing temperature is a critical point to obtain an optimum between an homogeneous sample having a high RIT.

It has been proved over the past decades that the use of appropriate doping agents can decrease the grain size of sintered alumina and thus improve the RIT. Conventional sintering at 1350 °C for 2 h under static air was performed on 4 non-thermally pre-treated freeze-dried alumina powders: pure alumina and alumina doped with Mg^{2+}, Zr^{4+} and La^{3+} nitrates. The relative density of the undoped ceramic was 93.8 ± 0.5%. For MgO doped ceramics, a regular increase of density was observed (93.7 ± 0.3%, 94.3 ± 0.4% and 95.7 ± 0.5% for 150, 300 and 500 ppm respectively). With ZrO_2 and La_2O_3, the inverse effect was noted: for 500 ppm ZrO_2 and La_2O_3 the density was 92.3 ± 0.5% and 93.1 ± 0.8% respectively. These results indicate that MgO doping enhances the densification whereas ZrO_2 and La_2O_3 reduce it at this sintering temperature. These results were confirmed by the dilatometric measurements that show that the densification of the ZrO_2 and La_2O_3-doped samples begins at higher temperatures than that of MgO-doped and undoped alumina samples (Fig. 4). The densification of the MgO-doped samples began at nearly the same temperature as that of undoped samples but the shrinkage of MgO-doped ceramic was greater above 1280 °C. The later of densification of ZrO_2 and La_2O_3-containing samples is explained by the segregation of the doping agents at grain boundaries (in solid solution and/or as precipitates). Indeed some works have already reported this segregation for all the doping agents considered [10,12,27–31] during conventional sintering. Thus, the diffusion of the Al ions is reduced and grain boundary sliding is limited. The result is controlled grain growth with densification at higher temperatures. This effect depends on the amount of doping agents included: as the dosage of doping agent decreased, the shrinkage curves became closer to those of undoped samples.

According to these results, optimizing the final temperature during the "SPS cycle" for each doping agent is necessary to achieve fully dense pellets.

3.2. Effect of thermal pre-treatment of the powder

Powders obtained by freeze-drying were thermally pre-treated at temperatures corresponding to the thermal decomposition of the doping element salts (nitrates or chlorides) to yield oxides, i.e. 450, 500, 650 and 700 °C for Mg (nitrate), Zr (nitrate and chloride), La (nitrate and chloride) and Mg (chloride) respectively, with no holding time. Preliminary thermal pre-treatment at 200 °C showed no influence on the specific surface areas (SSA) of powders which remained in the same range as those of non-thermally treated powders, 19–20 $m^2\,g^{-1}$. Lower SSA, between 14 and 16 $m^2\,g^{-1}$ were obtained after thermal pre-treatment at 650 °C without dwell. Thermal pre-treatment at 700 °C with 1 h dwell time weakly

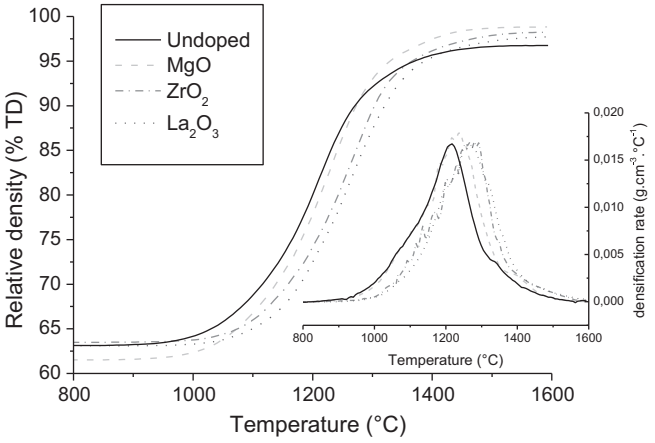

Fig. 4. Dilatometric measurements under air of 500 ppm doped alumina powders (MgO, ZrO_2, La_2O_3) prepared with nitrate salts.

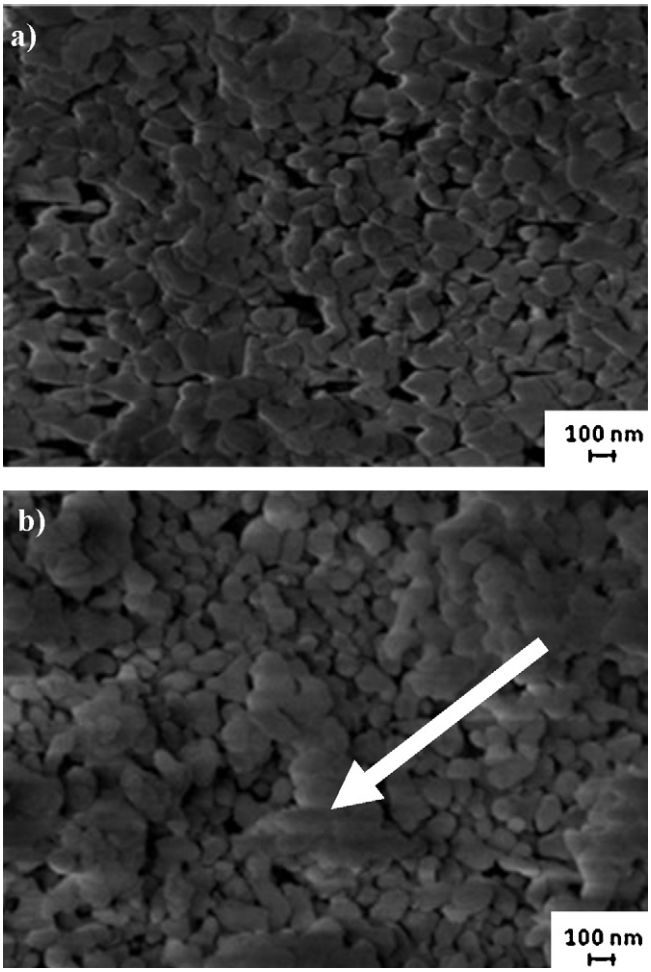

Fig. 5. SEM pictures of the freeze-dried 500 ppm MgO-doped alumina powder (a) non-thermally pre-treated (b) thermally pre-treated at 700 °C for 1 h.

decreased the SSA to 12–13 $m^2\ g^{-1}$. SEM analyses showed that agglomeration appeared at this elevated temperature (Fig. 5). Porosity measurements by mercury infiltration were performed on 200 ppm ZrO_2-doped alumina powder (nitrate based) either thermally pre-treated at 500 °C or not (Fig. 6a). Both powders presented the same range of intra-granular porosity (20–60 nm) indicating the same primary particle arrangement. However, bigger inter-granular porosity was found on thermally pre-treated powder (10–300 μm) indicating the presence of larger agglomerates. The two kinds of powders (thermally pre-treated or not) were then uniaxially pressed at 50 MPa. Fig. 6b shows the subsequent results of mercury infiltration measurement. The larger agglomerates were no longer present in the thermally pre-treated sample after pressing but porosity (100 nm–1 μm) was larger than that measured for the non-thermally treated samples (<200 nm). It is well known that large pores are harder to remove during sintering than small ones.

Three samples (undoped, 500 ppm ZrO_2-doped and 500 ppm MgO-doped) were prepared with and without thermal pre-treatment at 650 °C. Nitrate salts were used for the doping. After sintering in a conventional furnace at 1350 °C, the relative densities of all thermally pre-treated samples were lower than those of the non-thermally treated samples. Thus, the density of the undoped samples fell from 93.8 ± 0.5% to 87.2 ± 0.2%, that of the MgO-doped samples from 95.7 ± 0.1 to 90.3 ± 0.4 and that of the ZrO_2-doped samples from 92.3 ± 0.5 to 84.6 ± 0.3. When thermally pre-treating the powder, densification occurred at the same temperature as non-thermally pre-treated powder (Fig. 7) but the density of the green body was higher for non-thermally pre-treated samples leading to an improvement of densification (higher relative density throughout densification). Furthermore the higher green body density for non-thermally pre-treated powder was in good agreement with the mercury infiltration porosity measurements. Agglomeration during thermal pre-treatment led to poor particle packing so the pores were harder to remove during sintering as explained by Azar et al. [32].

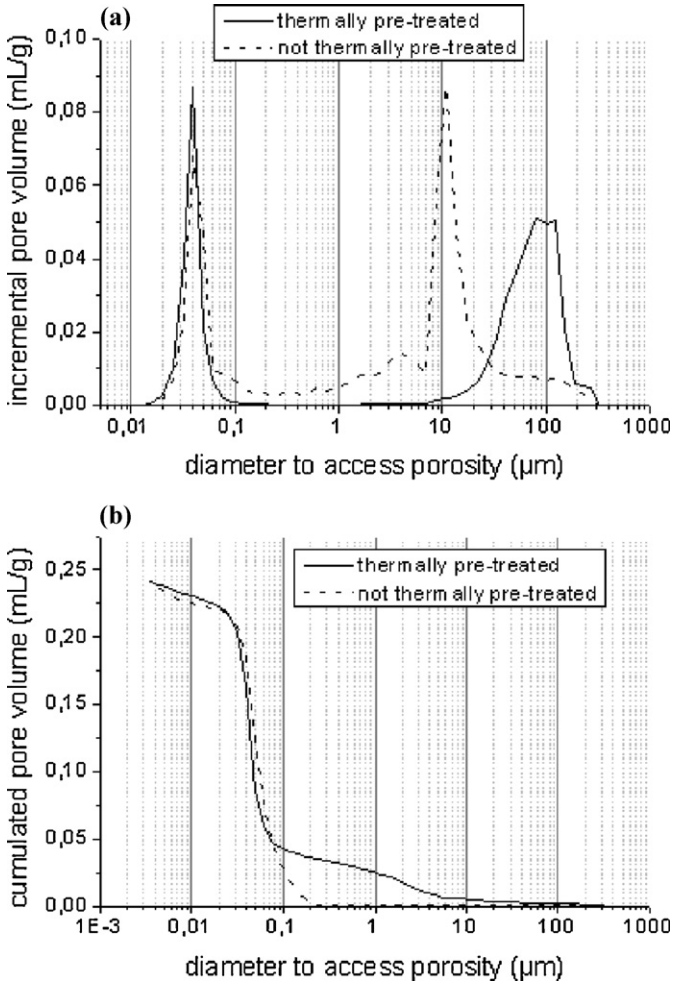

Fig. 6. Porosimetry measurement by mercury infiltration of a 200 ppm ZrO_2-doped alumina powder (nitrate) (a) incremental pore volume of the powder (b) cumulated pore volume after pressing (50 MPa).

3.3. Nitrate or chloride doping salt effect

Conventional sintering (1350 °C/2 h) was performed on 300 ppm MgO-doped alumina and 200 ppm ZrO_2-doped alumina, non thermally pre-treated. In both cases, two samples were prepared: one doped using the chloride salt and the other using the nitrate salt. The samples doped using chloride salts

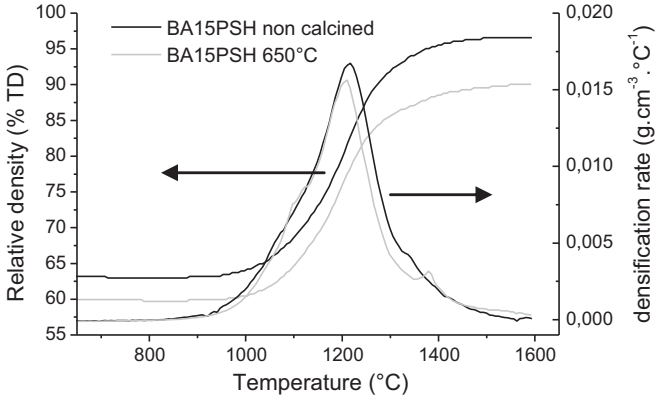

Fig. 7. Dilatometric measurements of pure freeze-dried alumina powders thermally pre-treated or not.

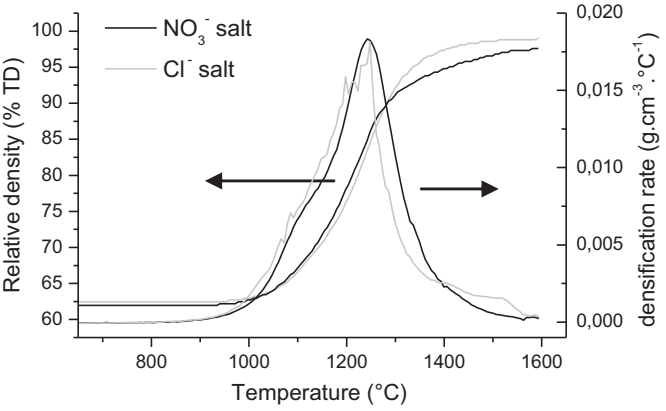

Fig. 8. Dilatometric measurement of non-thermally pre-treated alumina powders doped with 300 ppm of either Mg nitrate or chloride salt.

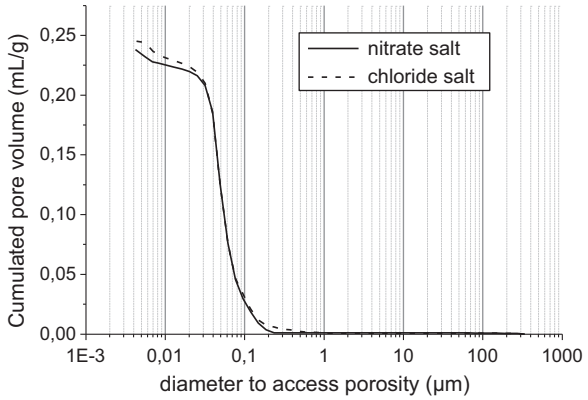

Fig. 9. Porosimetry measurement by mercury infiltration of non-thermally pre-treated 200 ppm ZrO_2-doped alumina powder (nitrate or chloride) – cumulated pore volume after pressing (50 MPa).

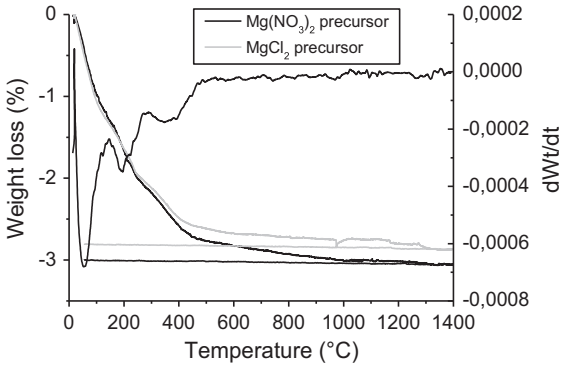

Fig. 10. Thermogravimetric measurements (TGA and DTG) of 2350 ppm MgO doped alumina (nitrate or chloride).

exhibit slightly higher densities than those doped using nitrate salts (96.1%TD against 94.3%TD for the MgO-doped alumina and 94.9%TD against 92.9%TD for the ZrO_2-doped alumina). The results are confirmed by the dilatometric curves (Fig. 8) as shown for the MgO-doped sample: sintering occurred at the same temperature for both salts (nitrate and chloride), while doping with chloride salt slightly improved the relative density at the end of sintering. Moreover, 200 ppm La_2O_3-doped non-thermally treated alumina powders prepared either with nitrate or chloride salts were sintered by SPS at a final temperature of 1280 °C. For λ = 640 nm and a thickness of 0.88 mm, the RIT measurement was slightly improved for the sample doped with chloride salt (48.1% against 45.9% for sample doped with nitrate salt). Since the samples were not thermally pre-treated, chloride or nitrate ions may have played a role during the sintering.

To understand the slightly better sintering behaviour of samples prepared with chloride salt, porosity was measured by mercury infiltration on 200 ppm ZrO_2-doped green bodies (non-thermally pre-treated powders were uniaxially pressed at

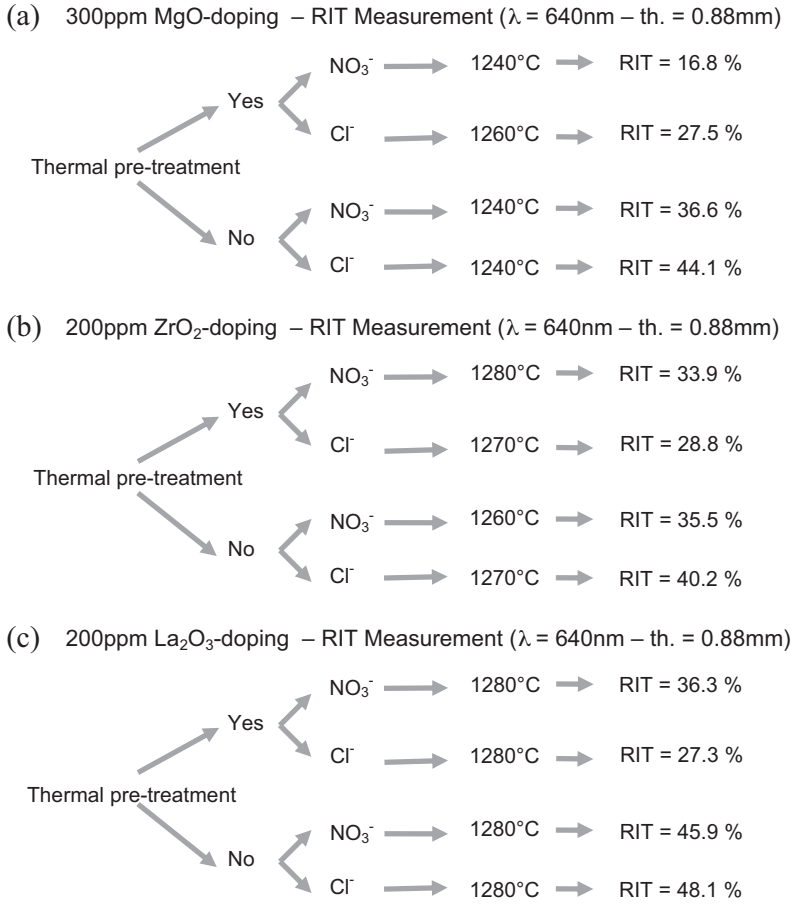

Fig. 11. RIT measurements (λ = 640 nm th = 0.88 mm) of (a) 300 ppm MgO-doped (b) 200 ppm ZrO_2-doped (c) 200 ppm La_2O_3-doped.

50 MPa) prepared either with nitrate or chloride salt. No significant difference was observed (Fig. 9) and sintering behaviour of powders doped with chloride salts cannot be explained by a better pressing behaviour or final packing homogeneity.

Thermogravimetric analysis under air at a heating rate of 2.5 °C/min was also performed on 2350 ppm MgO-doped, 7250 ppm ZrO_2-doped and 9650 ppm La_2O_3-doped alumina powders. Comparable behaviour was observed for the three doping elements. As shown in Fig. 10 for the MgO-doped samples, the chlorides and the nitrates are transformed into oxides in the same temperature range. The main part of the weight loss occurs during the three steps below 350 °C and then the weight slowly and regularly decreases until it reaches a constant value at about 1000 °C. The whole weight loss, close to 3 wt% was five to tenfold higher than that calculated for the transformation into oxide of the amount of doping chloride or nitrate, i.e. respectively 0.30 and 0.59 wt% for $MgCl_2$ and $Mg(NO_3)_2$. Below 250 °C, the two first losses are undoubtedly attributed to the release of adsorbed water and above 250 °C it is difficult to distinguish the end of dehydration and the start of decomposition of the doping salts. Although thermogravimetric investigation did not clarify the difference between nitrates and chlorides, doping with chloride salts enables slightly higher densities to be reached in natural sintering and a slightly better RIT after SPS sintering. Thus, it was decided to introduce doping elements into the slurry in the form of their chloride salt for the following steps of this study.

3.4. Sintering optimization of doped powders

Doped samples prepared with either chloride or nitrate salts (300 ppm MgO, 200 ppm ZrO_2, 200 ppm La_2O_3) either thermally pre-treated or not were sintered by SPS. Final sintering temperature was optimised for each doping agent as densification was delayed by their presence (fig. 4). RIT measurements were performed on these samples and the optimised results are given in Fig. 11. The results are in good agreement with those of the conventional sintering presented above. The SPS efficiency is also sensitive to the powder preparation, as previously shown in Section 3.2 for natural sintering. The presence of large agglomerates in the thermally pre-treated powder is detrimental to full densification of the ceramic. The residual porosity is associated to the former large inter-agglomerate pores, reducing the RIT value. Moreover, doping with chloride salt has slightly increased the RIT, as previously shown in Section 3.3, even though this effect was less pronounced than that of thermal pre-treatment. Finally, we were able to increase the RIT of doped-PCA up to 48.1% for La_2O_3-doped alumina.

The SEM micrographs of ceramics sintered at the optimised temperature for non-thermally pre-treated powders doped with chloride salts are reported in Fig. 12. All the doping agents led to a decrease in grain size (ϕ_G) compared to the freeze-dried pure alumina sintered at 1230 °C. (ϕ_G was equal to 1.17 ± 0.20, 0.63 ± 0.24, 0.79 ± 0.13, 0.81 ± 0.06 μm respectively for pure, MgO, ZrO_2, La_2O_3-doped alumina). However, the grain

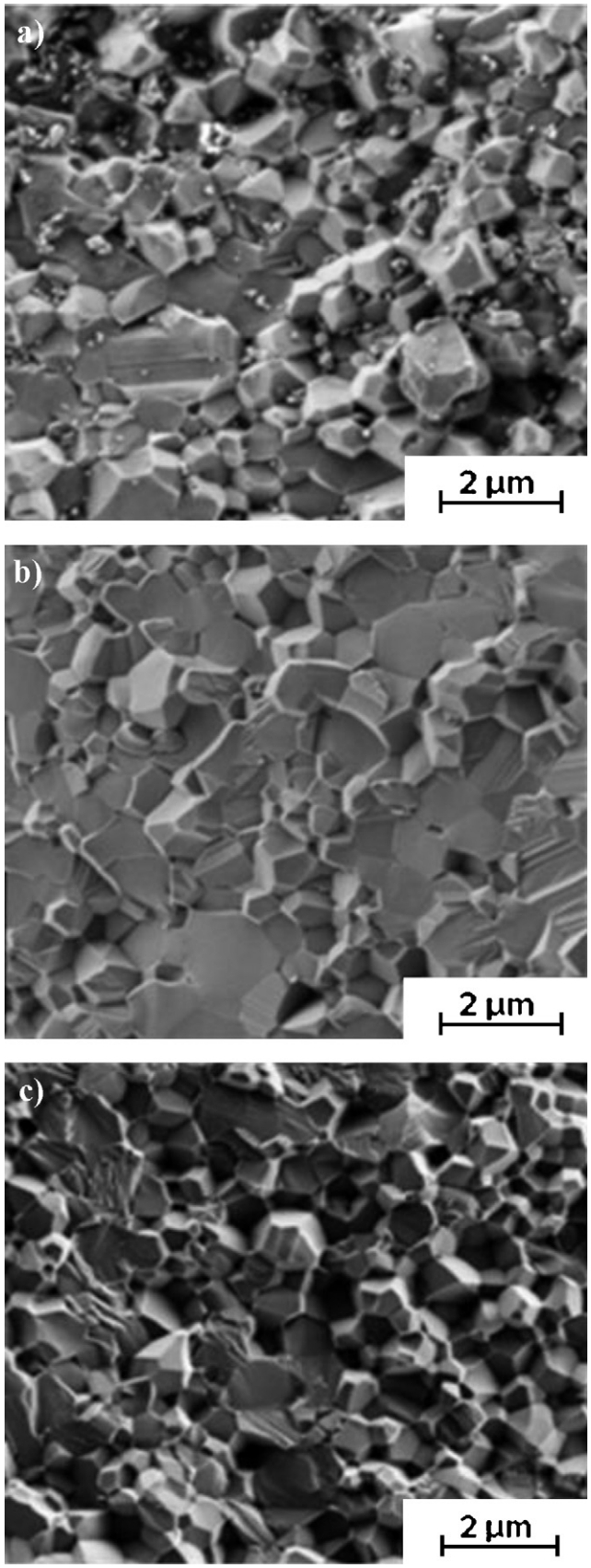

Fig. 12. SEM pictures of non-thermally pre-treated chloride based (a) 300 ppm MgO- (b) 200 ppm ZrO_2- (c) 200 ppm La_2O_3-doped alumina (sintering temperatures are optimised).

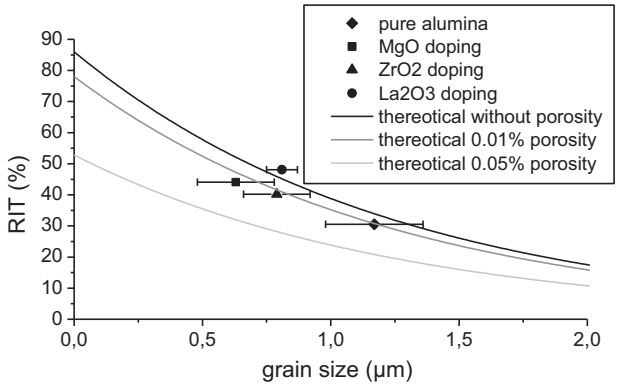

Fig. 13. Comparison of the RIT values of non-thermally pre-treated chloride based doped samples with the theoretical curves (λ = 640 nm th = 0.88 mm).

size was still heterogeneous even though an improvement occurred especially for the La_2O_3-doped sample. Moreover, the porosity remaining in these doped samples, except for La_2O_3 samples, was in the same range as that of optimized pure alumina at close to 0.01% (Fig. 13). Finally La_2O_3 seems to be more efficient than the other doping agents at increasing the RIT of PCA but the underlying reasons are still under investigation.

The RIT value found for the La_2O_3-doped sample is close to that found by Stuer et al. [5] (50% at 640 nm for a La_2O_3-doped sample with a thickness of 0.88 mm) with a 20-min SPS cycle (heating rate = 100 °C/min) and a final temperature of 1350 °C. The cycle used in our study lasted 4 h to obtain high density at low temperature. We attempted to reproduce Stuer's results using his specific thermal cycle, but no transparency was found with cycles at temperatures higher than the one we optimised. This can be explained by the amount of doping agent used. Stuer doped alumina with 3.6 times more La_2O_3 than we did, probably delaying the sintering over 1250–1300 °C. Another explanation can be found in the different size of the starting powder particles: around 5 times larger in Stuer's study. The higher particle size may delay sintering to higher temperatures.

Our RIT values can still be improved by optimizing the amount of each doping agent. This effect is currently under study.

4. Conclusion

Obtaining transparent polycrystalline alumina requires a very little amount of porosity and grains as fine as possible. This particular point can be achieved by both the use of doping agent and the SPS sintering technique for the densification of the sample as already published by Stuer et al. [5]. However, other parameters have to be optimised all over the process to avoid defects as agglomerates or porosity. In this study, the thermal pre-treatment, the nature of the doping salt and element and the sintering temperature have been investigated and their effects on the transparency of polycrystalline alumina (PCA) have been characterized. It has been shown that the sintering temperature has to be carefully optimised for each powder (doped or not) in order to obtain a homogeneous sample with a RIT as high as possible. Then, for doped samples, the thermal pre-treatment will lead to the formation of agglomerates, decreasing the specific surface areas and increasing sample inhomogeneity, making densification harder and lowering the resulting RIT. Moreover, doping with chlorides instead of nitrates can help to slightly improve densification in conventional sintering and lead to a slight improvement of the RIT by SPS sintering.

Finally, each doping agent enables to increase the RIT of PCA at 640 nm (40.1% for ZrO_2, 44.1% for MgO and 48.1% for La_2O_3 against 30.5% for pure alumina). If La_2O_3 appears to be the most efficient one, the reasons have not been determined yet and are still under investigation. Nevertheless, the results in this study should highlight the fact that each step of the process (from the powder preparation to the sintering of transparent polycrystalline alumina samples) has to be carefully optimised to avoid any defects as temperature/microstructure gradients, agglomeration or porosity which will induce a loss of RIT.

Acknowledgements

The authors are grateful for the financial support of the ANR CERATRANS and to all the participants, Lionel Bonneau (Baikowski), Johan Petit (ONERA), Stéphane Chaillot (BOOSTEC) and Denis Langlade (BTS Industrie).

References

[1] B.N. Kim, K. Hiraga, K. Morita, H. Yoshida, Effects of heating rate on microstructure and transparency of spark-plasma-sintered alumina, J. Eur. Ceram. Soc. 29 (2009) 323–327.
[2] A. Krell, J. Klimke, T. Hutzler, Advanced spinel and sub-μm Al_2O_3 for transparent armour applications, J. Eur. Ceram. Soc. 29 (2009) 275–281.
[3] A. Krell, T. Hutzler, J. Klimke, Transmission physics and consequences for materials selection, manufacturing, and applications, J. Eur. Ceram. Soc. 29 (2009) 207–221.
[4] A. Krell, J. Klimke, T. Hutzler, Transparent compact ceramics: inherent physical issues, Opt. Mater. 31 (8) (2009) 1144–1150.
[5] M. Stuer, Z. Zhao, U. Aschauer, P. Bowen, Transparent polycrystalline alumina using spark plasma sintering: effect of Mg, Y and La doping, J. Eur. Ceram. Soc. 30 (6) (2010) 1335–1343.
[6] R. Apetz, M.P.B. van Bruggen, Transparent alumina: a light-scattering model, J. Am. Ceram. Soc. 86 (3) (2003) 480–486.
[7] www.lightscattering.de/MieCalc/.
[8] S.J. Bennison, M.P. Harmer, Grain-growth kinetics for alumina in the absence of a liquid phase, J. Am. Ceram. Soc. 68 (1) (1985) C22–C24.
[9] S.J. Bennison, M.P. Harmer, Effect of MgO solute on the kinetics of grain growth in Al_2O_3, J. Am. Ceram. Soc. 66 (5) (1983) C90.
[10] A.M. Thompson, K.K. Soni, H.M. Chan, M.P. Harmer, D.B. Williams, J.M. Chabala, R. Levi-Setti, Dopant distributions in rare-earth-doped alumina, J. Am. Ceram. Soc. 80 (2) (1997) 373–376.
[11] K.K. Soni, A.M. Thompson, M.P. Harmer, D.B. Williams, J.M. Chabala, R. Levi-Setti, Solute segregation to grain boundaries in MgO-doped alumina, Appl. Phys. Lett. 66 (21) (1995) 2795–2797.
[12] J. Fang, A.M. Thompson, M.P. Harmer, H.M. Chan, Effect of yttrium and lanthanum on the final-stage sintering behavior of ultrahigh-purity alumina, J. Am. Ceram. Soc. 80 (8) (1997) 2005–2012.
[13] K.A. Berry, M.P. Harmer, Effect of MgO solute on microstructure development in Al_2O_3, J. Am. Ceram. Soc. 69 (2) (1986) 143–149.
[14] A.H. Chokshi, An evaluation of the grain-boundary sliding contribution to creep deformation in polycrystalline alumina, J. Mater. Sci. 25 (7) (1990) 3221–3228.

[15] J.D. Wang, R. Raj, Estimate of the activation energies for boundary diffusion from rate-controlled sintering of pure alumina, and alumina doped with zirconia or titania, J. Am. Ceram. Soc. 73 (5) (1990) 1172–1175.
[16] H. Yoshida, S. Hashimoto, T. Yamamoto, Dopant effect on grain boundary diffusivity in polycrystalline alumina, Acta Mater. 53 (2005) 433–440.
[17] B.N. Kim, K. Hiraga, K. Morita, H. Yoshida, Spark plasma sintering of transparent alumina, Scripta Mater. 57 (7) (2007) 607–610.
[18] B.N. Kim, K. Hiraga, K. Morita, H. Yoshida, T. Miyazaki, Y. Kagawa, Microstructure and optical properties of transparent alumina, Acta Mater. 57 (2009) 1319–1326.
[19] Z. Shen, et al., Spark plasma sintering of alumina, J. Am. Ceram. Soc. 85 (8) (2002) 1921–1927.
[20] Y. Aman, V. Garnier, E. Djurado, Spark plasma sintering kinetics of pure α-alumina, J. Am. Ceram. Soc. 94 (4) (2011).
[21] A. Krell, P. Blank, H. Ma, T. Hutzler, M. Nebelung, Processing of high-density submicrometer Al2O3 for new applications, J. Am. Ceram. Soc. 86 (4) (2003) 546–553.
[22] Y. Aman, V. Garnier, E. Djurado, Influence of green state processes on the sintering behaviour and the subsequent optical properties of spark plasma sintered alumina, J. Eur. Ceram. Soc. 29 (2009) 3363–3370.
[23] M.I. Mendelson, Average grain size in polycrystalline ceramics, JACS 52 (1969) 443–446.
[24] K. Vanmeensel, A. Laptev, J. Hennicke, J. Vleugels, O. Van der Biest, Modelling of the temperature distribution during field assisted sintering, Acta Mater. 53 (2005) 4379–4388.
[25] U. Anselmi-Tamburini, S. Gennari, J.E. garay, Z.A. Munir, Fundamental investigations on the spark plasma sintering/synthesis process II. Modelling of current and temperature distributions, Mater. Sci. Eng. A 394 (2005) 139–148.
[26] S. Muñoz, U. Anselmi-Tamburini, Temperature and stress field evolutions in spark plasma sintering, J. Mater. Sci. 45 (2010) 6528–6539.
[27] J.T. Lin, H.Y. Lu, Grain growth inhibition and mechanical property enhancement by adding ZrO_2 to Al_2O_3 matrix, Ceram. Int. 14 (1988) 251–258.
[28] D. Monceau, C. Petot, G. Petot-Ervas, J.W. Fraser, M.J. Graham, G.I. Sproule, Surface segregation and morphology of Mg-doped α-alumina powders, J. Eur. Ceram. Soc. 15 (1995) 851–858.
[29] H. Yoshida, Y. Ikuhara, T. Sakuma, Grain boundary electronic structure related to the high temperature creep resistance in polycrystalline Al_2O_3, Acta Mater. 50 (2002) 2955–2966.
[30] H. Yoshida, Y. Ikuhara, T. Sakuma, Vacancy effect of dopant cation on the high-temperature creep resistance in polycrystalline Al_2O_3, Mater. Sci. Eng. A 319–321 (2001) 843–848.
[31] J. Cho, M.P. Harmer, H.M. Chan, J.M. Rickman, A.M. Thompson, Effect of yttrium and lanthanum on the tensile creep behavior of aluminum oxide, J. Am. Ceram. Soc. 80 (4) (1997) 1013–1017.
[32] M. Azar, P. Palmero, M. Lombardi, V. Garnier, L. Montanaro, G. Fantozzi, J. Chevalier, Effect of initial particle packing on the sintering of nanostructured transition alumina, J. Eur. Ceram. Soc. 28 (2008) 1121–1128.